Macromolecules

Article

pubs.acs.org/Macromolecules

Effects of Temperature and Template Surface on Crystallization of Syndiotactic Polystyrene in Cylindrical Nanopores

Meng Li, Hui Wu, Yan Huang, and Zhaohui Su*

State Key Laboratory of Polymer Physics and Chemistry, Changchun Institute of Applied Chemistry, Chinese Academy of Sciences, Changchun 130022, P. R. China

Supporting Information

ABSTRACT: Crystallization of syndiotactic polystyrene (sPS) in anodized aluminum oxide (AAO) templates is investigated by FTIR. Nanopore surfaces of AAO templates are modified with *n*-hexyltrimethoxysilane to produce templates with alkyl surfaces, and effects of crystallization temperature and surface property of the template on the degree of crystallinity of sPS in nanopores of various sizes are studied. When isothermally crystallized at 245−260 °C, while the crystallinity in the bulk barely varies, in pristine and modified nanopores it increases substantially with degree of supercooling, which may be attributed to more surface-induced crystallization at lower temperatures. For all crystallization temperatures and pore sizes studied, sPS exhibits much lower crystallinity in the surface-modified templates, likely due to suppression of surface nucleation by the lower energy surfaces. This work reveals the significant role surface plays in polymer crystallization in nanotemplates and may aid the design and fabrication of polymeric nanodevices with well-defined structure and properties.

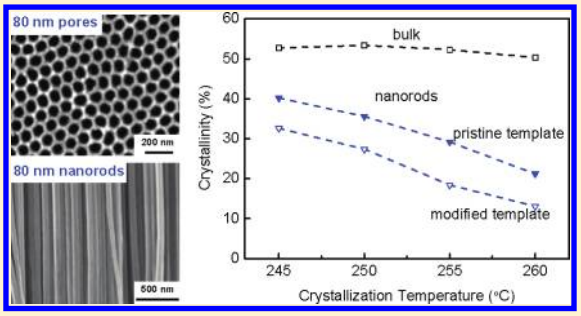

INTRODUCTION

Polymer crystallization under 2-dimentional (2D) confinement has aroused increasing interest in recent years.[1−7] For semicrystalline polymers, their physical properties are mainly governed by the crystalline domains; therefore, understanding their crystallization behavior under 2D confinement is of great significance in the design and development of nanorods and nanowires for microelectronics, optical, mechanical, and biomedical devices.[8−12] Crystallization in cylindrical domains formed by microphase separation in semicrystalline block copolymers has been studied.[13,14] Compared to block copolymer systems, anodized aluminum oxide (AAO) membranes possessing straight, rigid, and monodisperse cylindrical nanopores are ideal templates for fabrication of polymer nanorods,[15,16] and in these nanopores both ends of the polymer chain could move freely.

Recent studies have revealed that polymer crystallization in 2D confinement can lead to structures different from that in the bulk. For example, Hu et al. investigated crystallization of poly(vinylidene fluoride) (PVDF) in nanotrenches and found that in full confinement the fast growth direction of the crystals is parallel to the trenches, and the polymer chains are perpendicular to the trench direction.[6] Li et al. investigated polyimide-confined nylon-6 nanofibers and reported that the parallel oriented chains in the as-spun fibers become perpendicular to the fiber direction after recrystallization from melt.[7] Perpendicular orientation of chains has also been reported for crystallization of PVDF,[1] syndiotactic polystyrene (sPS),[3] and polyethylene (PE)[5,17] in AAO templates of various sizes, and suppression of crystallinity was also observed, which was more severe with decreasing pore size. In addition, nanoconfinement can lead to coexistence of different crystal modifications[4] and disturb crystal transformation.[7] These experimental results have been ascribed to effects of nanoconfinement on nucleation and growth behavior of the polymer crystals. Nuclei formed in the bulk reservoir connecting with the nanostructure grow into spherulites that would hit the nanopores, and only the lamellae with predominant growth direction conforming with the pore direction can grow into the nanopores, which is termed the "gate effect", leading to highly oriented crystals in the nanocylinders.[2] On the other hand, both heterogeneous nucleation and homogeneous nucleation can occur in polymer confined in nanopores; all crystal orientations occur with statistical frequency, but growth of the crystals with the orientations incompatible with pore direction is suppressed, which results in preferred orientation and lower crystallinity in the nanocynlinders.[7,18,19] At deep supercoolings large numbers of homogeneous nuclei are formed, and polymer in nanorods exhibits same degree of crystallinity as in the bulk, with no preferred crystal orientation.[4]

In addition to the factors described above, molecular simulation of polymer crystallization in rigid nanotubes has indicated that surface properties of the nanotube wall can significantly impact the crystallization within the nanopores.[20] Our recent experimental work on the orientation of sPS crystals in AAO templates of different pore diameters suggests that, in

Received: April 3, 2012
Revised: May 27, 2012
Published: June 11, 2012

addition to nuclei occurring in polymer in the bulk and in nanopores, surface-induced nucleation may play a role in the crystallization process.[21] In the present study, we modify the nanopore surface with alkylsilane and investigate the crystallization of sPS in AAO templates with different surface chemistries in order to explore experimentally the effects of surface properties on polymer crystallization under cylindrical confinement.

EXPERIMENTAL SECTION

Materials. Self-ordered AAO templates with average pore diameters of 32 and 80 nm were prepared via a two-step anodization process,[22,23] while templates with 200 nm pore diameter were purchased from Whatman. *n*-Hexyltrimethoxysilane (purity of >98%) was obtained from Gelest. sPS pellets (Questra F-2250, $M_w \sim 260\,000$, $M_w/M_n = 2$) were obtained from Dow Chemical Co. and used as received.

Modification of AAO Templates. AAO templates were modified following a literature procedure.[24] Dried AAO templates were placed in a homemade glass reactor under nitrogen atmosphere, and 0.5 mL of *n*-hexyltrimethoxysilane was injected by syringe into the reactor under nitrogen blanket without direct contact with the AAO templates.[25] The sealed reactor was transferred into an oven and maintained at 120 °C for 72 h to allow the silane vapor to react with the template surface. Then the treated templates were removed and ultrasonicated in toluene, ethanol, and water sequentially and dried in an oven at 120 °C for 15 min.

Sample Preparation. A pristine AAO membrane and a modified one were laid side-by-side on top of an amorphous sPS film, and the assembly was heated at 300 °C for 1 h under a nitrogen atmosphere so that the sPS melt was drawn into the nanopores by capillary force. Thermal degradation of the sPS in the process was insignificant (Supporting Information). The assembly was cooled from the molten state to a given crystallization temperature (260, 255, 250, and 245 °C) and annealed for 2 h, which has been shown to be sufficient for the crystallization process,[3] and then quenched in ice water quickly to freeze the structure formed at high temperatures. The template/polymer assembly was immersed in a sodium hydroxide aqueous solution to remove the AAO template, leaving nanorod arrays protruding from the bulk film. The length was about 60, 150, and 75 μm for the nanorods of 200, 80, and 32 nm diameter, respectively. Under an optical microscope thin slices of the cross section of the sPS film with protruding nanorods were cut using a razor blade for FTIR analyses.

Characterization. Water contact angles on the surfaces of pristine and modified AAO membranes were measured on a Ramè-Hart 200 standard goniometer using Milli-Q water (18.2 MΩ cm) as the probe fluid at 25 °C. Each contact angle value reported was an average of at least five independent measurements. X-ray photoelectron spectra (XPS) were acquired on a ThermoVG ESCALAB 250 spectrometer equipped with a monochromatic Al X-ray source (1486.6 eV). The spectra were recorded at a 90° takeoff angle with 20 eV pass energy. Scanning electron microscopy (SEM) observations were carried out on a FEG-SEM Hitachi S-4700 microscope operating at 20 kV. The samples were coated with a thin layer of gold before the SEM observations. FTIR spectra were recorded on a Bruker IFS 66 V/S spectrometer in connection with a Bruker Hyperion 3000 microscope equipped with a narrow band mercury–cadmium telluride (MCT) detector operating in transmission mode. The spectra were collected at 2 cm^{-1} resolution with 256 scans coadded. Curve fitting was performed using the Levenberg–Maquardt least-squares algorithm routine of the OPUS software package, and the residual rms error was lower than 0.002. The degree of crystallinity was calculated using the bands in the 870–820 cm^{-1} region via the equation[26]

$$C_\beta = \frac{A_{858}/a_\beta}{A_{841} + A_{851}/a_\alpha + A_{858}/a_\beta} \times 100\% \quad (1)$$

where C_β represents the β crystallinity and A_{841}, A_{851}, A_{858} are the band areas for amorphous and α- and β-crystals, respectively. Each number reported is an average of seven measurements.

RESULTS AND DISCUSSION

The alumina surfaces are rich in Al–OH groups, which afford a convenient handle for covalent attachment of various molecules for desired surface properties. Trimethoxysilanes can readily react with alumina surfaces,[27] and this reaction was employed here for alkylation of the pore surfaces in AAO templates. Since this is a vapor phase reaction and the silane molecule is very small compared to the pore size, the modification in the nanopores is expected to be same as that on the membrane surfaces. Table 1 lists water contact angle values and Si contents measured by XPS for AAO membranes modified by silanization with *n*-hexyltrimethoxysilane. The water contact angle of the AAO surfaces increases significantly after the modification from hydrophilic to hydrophobic, apparently due to conversion of the surface OH groups to the alkyl groups. Figure 1 compares the XPS survey spectra of the cross sections of a pristine AAO membrane and a modified one. The Si 2p peak at 102 eV, which is absent in the spectrum of the pristine AAO, is clearly identified for the modified AAO. The presence of Si element at the surfaces of the modified AAO further confirms the covalent attachment of the alkylsilane to the nanopore surfaces. The modified AAO membranes exhibited no change in water contact angle after being heated under vacuum at 300 °C for 1 h, indicating high thermal stability of the *n*-hexylsilane layer attached, which accords with that reported in literature.[28]

Table 1. Water Contact Angles for Pristine and Modified AAO Templates and Corresponding Si Content Measured by XPS

	water contact angle (deg)		
pore diam (nm)	pristine AAO	modified AAO	Si content (%)
200	16.8 ± 1.1	133.8 ± 1.6	4.7
80	62.8 ± 0.9	119.2 ± 1.8	3.4
32	58.7 ± 1.9	102.5 ± 0.9	3.1

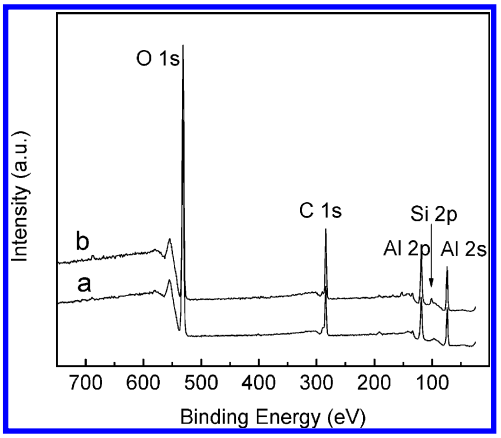

Figure 1. XPS survey spectra of the cross section of (a) pristine and (b) modified AAO templates of 80 nm pore size.

Then sPS nanorods were prepared using the nanoporous AAO membranes as templates. Figure 2 shows SEM images of pristine and modified AAO membranes of 80 nm pore diameter and the corresponding sPS nanorods obtained as an example. It

dx.doi.org/10.1021/ma300688h | Macromolecules 2012, 45, 5196–5200

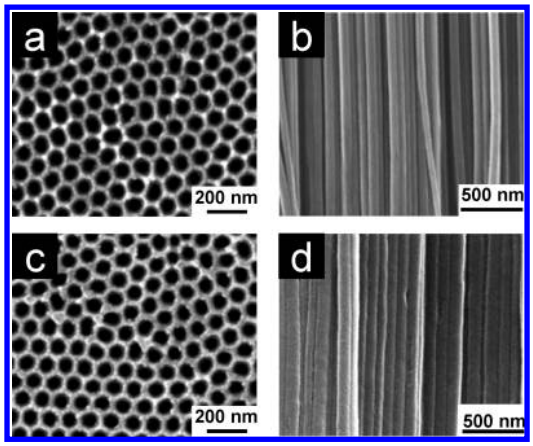

Figure 2. SEM images of (a) pristine and (c) modified AAO templates with pore size of 80 nm and (b, d) corresponding sPS nanorods prepared therefrom.

can be seen that the pore sizes are rather uniform, and the corresponding polymer nanorods are uniform in diameter and well aligned in the perpendicular direction. Next the sPS nanorods were analyzed by micro-FTIR. Vibrational bands characteristic of different morphologies of sPS are found in the 940−820 cm^{-1} region. More specifically, the bands at 901 and 851 cm^{-1} correspond to the α-form crystals, and the components at 911 and 858 cm^{-1} are correlated to the β-crystal modification, whereas the bands at 905 and 841 cm^{-1} are assigned to the amorphous phase.[29] Figure 3 displays as an

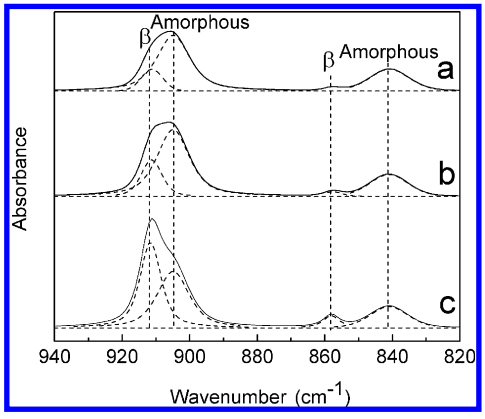

Figure 3. Representative IR spectra of sPS crystallized at 255 °C in the region of 940−820 cm^{-1} for 80 nm nanorods from (a) modified and (b) pristine templates and (c) bulk film beneath the nanorods. The dotted lines are the fitted results.

example a set of IR spectra in the 940−820 cm^{-1} region of sPS nanorods fabricated using pristine and modified AAO templates of 80 nm pore size as well as the bulk film allowed to crystallize at 255 °C, with curve fitting results. IR spectra for other pore sizes and crystallization temperatures are included in the Supporting Information. The data clearly indicate the presence of amorphous phase and β-form crystals and the absence of α-crystal modification. Similar results were obtained for other crystallization temperatures, of 245 °C or above. This is consistent with our previous findings.[4] The areas of these curve-fitted peaks were then used to calculate degree of crystallinity[26] in the nanorods as well as in the bulk. The results are plotted in Figure 4.

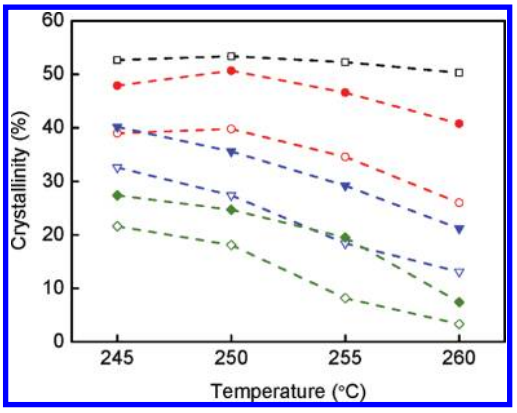

Figure 4. Degree of crystallinity as a function of crystallization temperature for nanorods crystallized in pristine (solid symbols) and modified (empty symbols) templates with different pore sizes (red circles, 200 nm; blue triangles, 80 nm; green diamonds, 32 nm), with that for the bulk (black squares) as a comparison. The dashed lines are to guide the eye.

First, it can be seen that for the crystallization temperature range investigated, 245−260 °C, sPS nanorods exhibit significantly lower degree of crystallinity than the bulk, and for any particular crystallization temperature, the degree of crystallinity decreases with the diameter of the nanorods. For example, for sPS isothermally crystallized at 260 °C, the crystallinity is 41, 21, and 7% respectively in pristine templates with pore sizes of 200, 80, and 32 nm, all much lower than that in the bulk, 52%. The same trend is observed for sPS nanorods grown in both pristine and modified templates and is consistent with our previous report.[3] This depression in crystallinity is attributed to the geometric confinement imposed by the nanopore walls on the growth of lamellar crystals initiated by the few heterogeneous nuclei in the tiny volume of individual nanopores (more details below) and the "gate effect" on the growth of lamellae from the bulk into the nanopores.[3,4] Next we notice that in nanorods the degree of crystallinity increases with supercooling. For example, for nanorods grown in pristine template of 80 nm pore size, the crystallinity is 21, 29, 36, and 40% when crystallized at 260, 255, 250, and 245 °C, respectively. In contrast, in the bulk the crystallinity remains fairly constant over the wide temperature range, which is consistent with the finding by Strobl et al. in their study on crystallization of syndiotactic polypropylene and its copolymers that fully developed crystallinity remains invariant over a large crystallization temperature range.[30] It has been reported that homogeneous nucleation is negligible in sPS at crystallization temperatures of 230 °C and higher[4] and therefore plays no role in this study. In a separate experiment, isothermal crystallization of sPS at 245 and 260 °C in thin films was observed by a polarized optical microscope, and the average size of the spherulites was found to be roughly the same at 7.4 μm for both crystallization temperatures (data not shown). This result indicates that the density of heterogeneous nuclei is not affected by temperature. In addition, we can estimate that the density of heterogeneous nuclei is $\sim 2.5 \times 10^{-3}/\mu m^3$, and the probability of finding one nucleus in each of the nanopores is $(0.1-5) \times 10^{-3}$, depending on the pore diameter. Therefore, the contribution of heterogeneous nuclei within the nanopores is negligible. On the other hand, crystallization induced by the nanopore walls[21] may be enhanced at lower temperatures, which probably is responsible for the crystallinity dependency

dx.doi.org/10.1021/ma300688h | Macromolecules 2012, 45, 5196−5200

on crystallization temperature we observe here for all the sPS nanorods.

Lastly, we investigate the effects of surface properties of the templates on sPS crystallization in the nanopores. From Figure 4 it can be observed that at any given crystallization temperature and pore size nanorods obtained from AAO template with alkane surface exhibit significantly lower crystallinity than that from pristine template. Because the *n*-hexyl group is short, the *n*-hexylsilane monolayer attached to the surfaces of the nanopores is very thin and does not alter the pore geometry significantly, so the surface modification does not expect to impact the crystals grown from the heterogeneous nuclei in the nanopores as well as from the bulk film through the "gates". Since bulk homogeneous nucleation is excluded based on the crystallization temperature, the difference in crystallinity observed between nanorods from pristine and modified templates can only be attributed to surface influenced crystallization, which was suggested by previous experiments to be present in sPS crystallization in AAO templates.[21] In fact, Chartterjee et al.[31] reported the relationship between surface nucleation and interfacial energy for different substrates long time ago. The quantity $(\sigma_m - \sigma_c)$ can be used to represent the nucleating ability of a substrate, where σ_m is the substrate−melt interfacial energy and σ_c is the substrate−crystal interfacial energy. A higher value of $(\sigma_m - \sigma_c)$ indicates a better heterogeneous nucleating ability. Despite the fact that σ_c values have neither been directly measured nor indirectly calculated, relative to melt spreading, forming a unit area of substrate−crystal interface consumes rather less energy. Thus, for a particular polymer, wettability should reflect the heterogeneous nucleation ability of the substrate surface. Obviously, the surface energy of the alkyl-modified templates is much lower than that of the pristine alumina, and sPS melt wets the high-energy pristine alumina surface much more easily than the alkyl-modified template surface. Therefore, in the nanopores with alkyl surfaces, nucleation of sPS chains at the pore surfaces is significantly suppressed; surface-induced nuclei tend to be parallel to the long axis of the pore, and less amount of such edge-on crystals will block the development of crystallinity along the pore,[20] resulting in much lower crystallinity compared to that in pristine AAO templates. This result indicates that surface-induced crystallization contributes significantly to the crystallinity in sPS nanorods prepared using AAO templates. Averaged over the temperatures studied, the crystallinity difference between the nanorods prepared from the two kinds of templates accounts for roughly 26, 30, and 40% of the sPS crystallinity in pristine templates of 200, 80, and 32 nm size, respectively, the trend correlating well with the increasing surface-to-volume ratio for the nanopores.

CONCLUSIONS

In this work, we have modified the nanopore surfaces of AAO template and investigated crystallization of sPS in cylindrical nanopores with different surface chemistries, in particular effects of crystallization temperature and pore size on the degree of crystallinity in pristine and modified templates. While in the bulk the sPS crystallinity remains independent of crystallization temperature, in nanopores it increases with degree of supercooling, probably due to more surface-induced crystallization at lower temperatures. In alumina nanopores surface-modified with an alkyl monolayer, the degree of crystallinity is greatly reduced compared to that in the pristine alumina templates, attributable to suppression of surface nucleation by the lower energy surface of the modified nanotemplates. These results indicate that surface-induced crystallization can play a significant role in crystallization in polymer nanorods. This work provides new insights into polymer crystallization in nanotemplates and may aid the design and fabrication of polymeric nanodevices with well-defined structure and properties.

ASSOCIATED CONTENT

Supporting Information

IR spectra for all pore sizes and crystallization temperatures, SEM image of a thin slice of nanorod array/bulk film, and sPS molecular weight data. This material is available free of charge via the Internet at http://pubs.acs.org.

AUTHOR INFORMATION

Corresponding Author

*Ph (+86)431-85262854; Fax (+86)431-85262126; e-mail zhsu@ciac.jl.cn.

Notes

The authors declare no competing financial interest.

ACKNOWLEDGMENTS

This work was supported by the National Natural Science Foundation of China (20774097). Z.S. thanks the NSFC Fund for Creative Research Groups (50921062) for support.

REFERENCES

(1) Steinhart, M.; Senz, S.; Wehrspohn, R. B.; Gösele, U.; Wendorff, J. H. *Macromolecules* **2003**, *36*, 3646.
(2) Steinhart, M.; Göring, P.; Dernaika, H.; Prabhukaran, M.; Gösele, U.; Hempel, E.; Thurn-Albrecht, T. *Phys. Rev. Lett.* **2006**, *97*, 027801.
(3) Wu, H.; Wang, W.; Yang, H.; Su, Z. *Macromolecules* **2007**, *40*, 4244.
(4) Wu, H.; Wang, W.; Huang, Y.; Wang, C.; Su, Z. *Macromolecules* **2008**, *41*, 7755.
(5) Shin, K.; Woo, E.; Jeong, Y. G.; Kim, C.; Huh, J.; Kim, K.-W. *Macromolecules* **2007**, *40*, 6617.
(6) Hu, Z.; Baralia, G.; Bayot, V.; Gohy, J.-F.; Jonas, A. M. *Nano Lett.* **2005**, *5*, 1738.
(7) Liu, Y.; Cui, L.; Guan, F.; Gao, Y.; Hedin, N. E.; Zhu, L.; Fong, H. *Macromolecules* **2007**, *40*, 6283.
(8) Martin, C. R. *Acc. Chem. Res.* **1995**, *28*, 61.
(9) Jang, J. *Adv. Polym. Sci.* **2006**, *199*, 189.
(10) Arinstein, A.; Zussman, E. *J. Polym. Sci., Part B: Polym. Phys.* **2011**, *49*, 691.
(11) Liang, D.; Hsiao, B. S.; Chu, B. *Adv. Drug Delivery Rev.* **2007**, *59*, 1392.
(12) Barnes, C. P.; Sell, S. A.; Boland, E. D.; Simpson, D. G.; Bowlin, G. L. *Adv. Drug Delivery Rev.* **2007**, *59*, 1413.
(13) Huang, P.; Zhu, L.; Cheng, S. Z. D.; Ge, Q.; Quirk, R. P.; Thomas, E. L.; Lotz, B.; Hsiao, B. S.; Liu, L.; Yeh, F. *Macromolecules* **2001**, *34*, 6649.
(14) Nojima, S.; Ohguma, Y.; Kadena, K.-i.; Ishizone, T.; Iwasaki, Y.; Yamaguchi, K. *Macromolecules* **2010**, *43*, 3916.
(15) Li, A. P.; Muller, F.; Birner, A.; Nielsch, K.; Gosele, U. *J. Appl. Phys.* **1998**, *84*, 6023.
(16) Martin, C. R. *Science* **1994**, *266*, 1961.
(17) Wu, H.; Wang, W.; Su, Z. H. *Acta Polym. Sin.* **2009**, *5*, 425.
(18) Woo, E.; Huh, J.; Jeong, Y. G.; Shin, K. *Phys. Rev. Lett.* **2007**, *98*, 136103.
(19) Duran, H.; Steinhart, M.; Butt, H.-J. r.; Floudas, G. *Nano Lett.* **2011**, *11*, 1671.
(20) Ma, Y.; Hu, W.; Hobbs, J.; Reiter, G. *Soft Matter* **2008**, *4*, 540.
(21) Wu, H.; Wang, W.; Huang, Y.; Su, Z. *Macromol. Rapid Commun.* **2009**, *30*, 194.

(22) Masuda, H.; Fukuda, K. *Science* **1995**, *268*, 1466.
(23) Sauer, G.; Brehm, G.; Schneider, S.; Nielsch, K.; Wehrspohn, R.; Choi, J.; Hofmeister, H.; Gösele, U. *J. Appl. Phys.* **2002**, *91*, 3243.
(24) Stafford, C. M.; Fadeev, A. Y.; Russell, T. P.; McCarthy, T. J. *Langmuir* **2001**, *17*, 6547.
(25) Silberzan, P.; Leger, L.; Ausserre, D.; Benattar, J. J. *Langmuir* **1991**, *7*, 1647.
(26) Wu, H.-D.; Wu, I. D.; Chang, F.-C. *Macromolecules* **2000**, *33*, 8915.
(27) Vlassiouk, I.; Krasnoslobodtsev, A.; Smirnov, S.; Germann, M. *Langmuir* **2004**, *20*, 9913.
(28) Kulkarni, S. A.; Mirji, S. A.; Mandale, A. B.; Vijayamohanan, K. P. *Thin Solid Films* **2006**, *496*, 420.
(29) Musto, P.; Tavone, S.; Guerra, G.; De Rosa, C. *J. Polym. Sci., Part B: Polym. Phys.* **1997**, *35*, 1055.
(30) Strobl, B. H.; Hugel, T.; Iijima, M.; E Sadiku, G. *New J. Phys.* **1999**, *1*, 17.
(31) Chatterjee, A. M.; Price, F. P.; Newman, S. *J. Polym. Sci., Polym. Phys. Ed.* **1975**, *13*, 2391.